Al^{3+} ion storage behavior of $LiFePO_4$ in aqueous electrolyte

6.1 Introduction

This chapter investigates the probable Al^{3+}-ion intercalation/deintercalation in lithium iron phosphate ($LiFePO_4$) in different Al^{3+}-ion conducting aqueous electrolytes. Goodenough and his co-workers first demonstrated the Li^+-ion storage in phospho-olivines in nonaqueous electrolyte in the year 1997 [1]. $LiFePO_4$ swiftly proliferated from laboratory scale research to commercial platform with the advent of LFP battery. $LiFePO_4$ is an important cathode material for lithium-ion batteries because it avoids toxic and scare cobalt with environment friendly and abundant iron species. It exhibits flat charge-discharge profiles at a potential of 3.4 V (vs. Li^+/Li) with little polarization. The specific theoretical capacity of $LiFePO_4$ is 170 $mAhg^{-1}$. Most of the studies on $LiFePO_4$ were performed in non-aqueous electrolyte. It is interesting to note that the Li^+-ion electrochemistry of $LiFePO_4$ in aqueous electrolyte shows contrasting behavior in comparison to nonaqueous electrolyte. There are only few reports on the aqueous Li^+-ion electrochemistry of $LiFePO_4$ for rechargeable aqueous batteries [2, 3-9]. Recently, our group also studied the Al^{3+}-ion electrochemistry of $LiMn_2O_4$ in aqueous electrolyte and this study unveils several strange but interesting facts which are uncommon in non-aqueous system [10]. For example, it was found that $LiMn_2O_4$ converts to amorphous and crystalline phases of MnO_2 during cycling and the cycling stability could be significantly improved by optimization of the electrolyte by incorporating Mn^{2+}-ions [10]. In this particular chapter, an attempt has been made to unravel the Al^{3+}-ion electrochemistry in $LiFePO_4$ since nothing is known about it to the best of our knowledge.

6.2 Experimental

6.2.1 Materials: Lithium iron phosphate ($LiFePO_4$) was directly purchased from SRL chemical. Aluminium chloride hexahydrate (Merck), aluminium sulphate 16-hydrate (Merck), aluminium nitrate monohydrate (Merck), lithium sulphate monohydrate (SRL), hydrochloric acid (Merck), carbon black (Alfa Aesar) and polyvinylidene fluoride (Sigma Aldrich) and N-methyl-2-pyrrolidone (Alfa Aesar) have been used for performing the electrochemical experiments.

6.2.2 Electrode preparation and electrochemical measurement: $LiFePO_4$ was directly used without any further treatment for the electrochemical analysis. Electrode slurries were prepared by thoroughly mixing $LiFePO_4$, carbon black and PVDF in mass ratio of 75:15:10 in NMP as medium. Then the slurry was drop coated on Ti foil (1 cm x 1 cm) and finally dried in an oven at 100 ^oC for 12 h. The mass loading in the prepared electrodes was approximately in the range of 5-6 mg. Cyclic voltammetry (CV) and galvanostatic charge/discharge (GCD) measurements were carried out in three electrodes arrangement in AUTOLAB 302N Potentiostat/Galvanostat. The three electrodes were: 1 M KCl electrolyte containing aqueous Ag/AgCl as reference electrode, platinum rod (3 mm diameter) as counter electrode and active material deposited Ti foil as working electrode. CV and GCD were performed in various aqueous electrolytes in the potential window of -0.8 to 1 V unless otherwise stated. Specific capacity (C_{sp}) was calculated using the following equation [6.1]:

$$C_{sp} = \frac{I\Delta T_d}{m} \qquad [6.1]$$

where I, ΔT_d and m are constant discharge/charge current, discharge period, and mass loading in the prepared electrodes respectively. All the electrochemical experiments were performed at room temperature.

6.2.3 Structural and morphological characterizations: Powder X-ray diffraction (P-XRD) measurements were performed for crystallographic phase identification using D8 focus X-ray diffractometer (Cu-Kα radiation, λ = 1.5406 Å), Bruker AXS at a scanning rate of 1^o min^{-1} in 2θ range of 15-80^o. The surface morphology of the electrodes was observed by field emission scanning electron microscopy (FESEM, JEOL JSM 7200F). XPS was carried out in Physical Electronics PHI 5000 Versa Probe III C_{60} ion gun.

6.3 Results and discussion

The microstructure and morphology of $LiFePO_4$ were investigated by X-ray diffraction and electron microscopy techniques. XRD pattern of $LiFePO_4$ is depicted in figure 6.1 a. The XRD peaks at 2θ = 17.28, 20.83, 22.76, 24.17, 25.70, 29.95, 32.38, 35.85^o correspond to the planes (200), (101), (210), (011), (201), (020), (301) and (311) respectively [JCPDS # 83-2092, space group Pnma]. The sharp XRD peak indicates the crystalline nature of $LiFePO_4$. From SEM micrograph (figure 6.1 b),

flake like $LiFePO_4$ particles could be observed with a broad size distribution in the range of 200 nm to 1 µm.

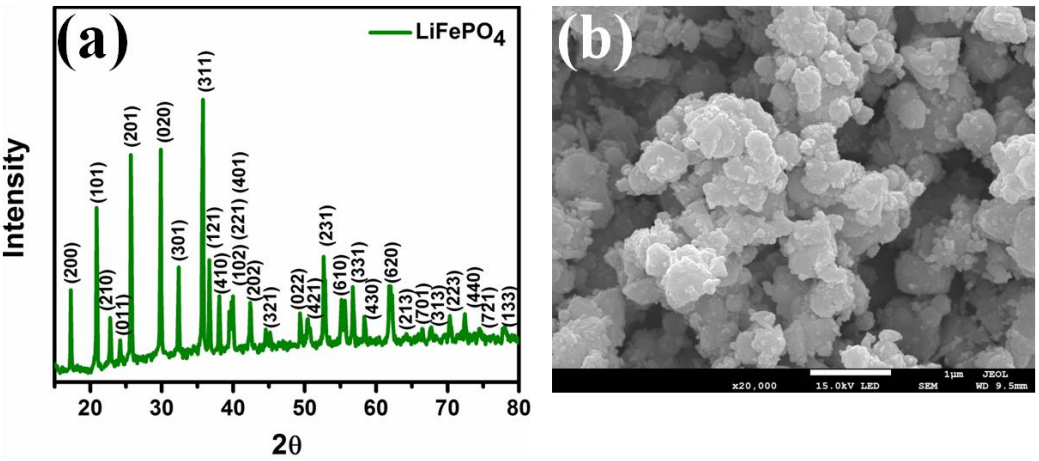

Figure 6.1: (a) XRD pattern and (b) FESEM of $LiFePO_4$

The electrochemical activity of $LiFePO_4$ in Li^+-ion conducting aqueous electrolyte has been investigated previously [3-9]. Therefore, to ascertain a consistent outcome, we initially explored the Li^+ ion electrochemistry of $LiFePO_4$ in 0.5 M Li_2SO_4 aqueous electrolyte to observe the process of Li^+-ion intercalation/deintercalation. Figure 6.2 a shows the cyclic voltamogram of $LiFePO_4$ at a scan rate of 1 mVs^{-1} and redox behavior is easily noticeable. A pair of prominent redox peaks could be seen in the cyclic voltammetry measurements. The cathodic and anodic peaks are observed at around -0.16 V and 0.46 V (vs. Ag/AgCl) respectively. The galvanostatic charge/discharge (GCD) measurement (Figure 6.2 b) also supports the cyclic voltammetry result. The GCD measurement was performed at a current density of 0.3 Ag^{-1}. The discharge curves show a plateau around 0.12 V (vs. Ag/AgCl), whereas the charge curves show the plateau at 0.25 V suggesting the intercalation/deintercalation of Li^+-ions in $LiFePO_4$. The CV and charge/discharge experimental outcomes are in corroboration with previous reports [11]. This supports that the selected $LiFePO_4$ could be used for our further studies. In the present case, the estimated discharge capacity of $LiFePO_4$ is 157 $mAhg^{-1}$ in the first cycle. There is gradual decrease in specific capacities and the electrode could retain only 28% of specific capacity in the 20^{th} cycle. It is a well-known fact that $LiFePO_4$ shows severe capacity decline in Li^+-ion conducting aqueous electrolytes [11].

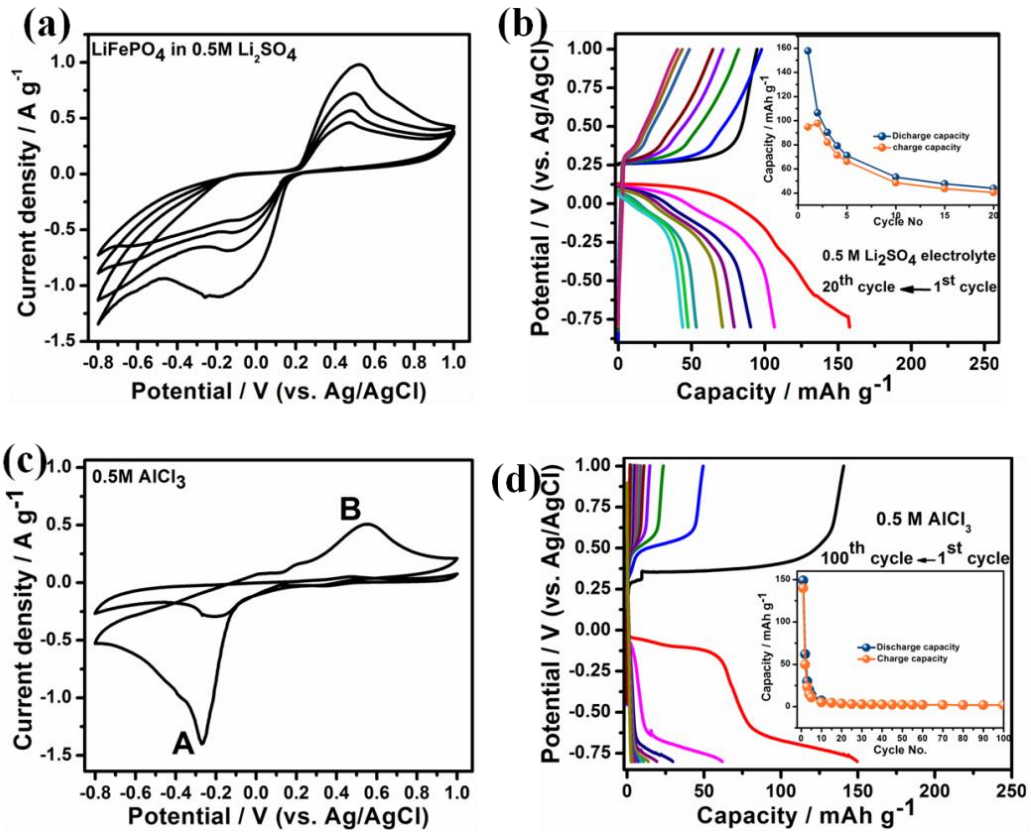

Figure 6.2: Electrochemical measurements of $LiFePO_4$. (a) Cyclic voltammetry (CV) at scan rate of 1 mVs^{-1}, (b) galvanostatic charge-discharge (GCD) profile at current density of 0.3 Ag^{-1} for 20 repeated cycles (inset shows capacity vs. cycle number plot) in 0.5 M Li_2SO_4 aqueous electrolyte; and (c) CV at scan rate of 1 mVs^{-1} and (d) GCD at current density of 0.3 Ag^{-1} for 20 repeated cycles (inset shows capacity vs. cycle number plot) in 0.5 M $AlCl_3$ aqueous electrolyte.

Based on the outcome of Li^+-ion electrochemistry, the electrochemical activity of $LiFePO_4$ was exclusively investigated in Al^{3+}-ion conducting aqueous electrolytes. Figure 6.2 c shows the CV profile of $LiFePO_4$ in 0.5 M $AlCl_3$ aqueous electrolyte at a scan rate of 1 mVs^{-1}. Two prominent redox peaks could be observed. The cathodic and anodic peaks are at -0.26 V (peak A) and 0.55 V (peak B) respectively. The potential is measured w.r.t. Ag/AgCl reference electrode. The charge/discharge profiles obtained at a current density of 0.3 Ag^{-1} also show discharge and charge potential plateaus around -0.08 V and 0.35 V respectively (Figure 6.2 d), which is fairly in consistent with the redox peak positions as observed in the corresponding CV profiles. It is noted that the charge plateau shifts to 0.5 V in subsequent charge cycles. $LiFePO_4$ initially exhibits high specific capacity of 140 $mAhg^{-1}$ and 149 $mAhg^{-1}$

respectively in the 1st charge and 2nd discharge cycle, however there is severe decline of specific capacities with progressing cycle number similar to our earlier discussed Li^+-ion study. The discharge capacity is only 3.53 $mAhg^{-1}$ at the 20th cycle. Following the similar protocol as was reported for $LiMn_2O_4$, we performed the discharge first. The 1st discharge cycle capacity is found to be small (11 $mAhg^{-1}$) (Figure 6.3).

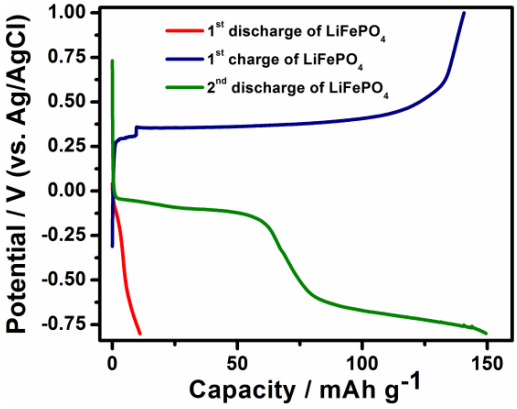

Figure 6.3: 1st discharge, 1st charge and 2nd discharge GCD pattern of $LiFePO_4$ in 0.5 M $AlCl_3$ aqueous electrolyte at current density of 0.3 Ag^{-1}.

We also investigated the Al^{3+}-ion electrochemistry in electrolytes with different molar concentrations. Electrochemical activity of varying degrees could be seen from the CV profiles in all the investigated electrolytes (0.1 M, 0.25 M and 1 M $AlCl_3$ aqueous electrolytes) as shown in Figure 6.4. However, charge-discharge profiles with significant specific capacities could be achieved only with 0.25 M electrolyte. The discharge capacity is 28 $mAhg^{-1}$ at current density of 0.3 Ag^{-1} in the initial cycle. On the other hand, the initial discharge measurement could not be even completed at the similar current density for 1 M $AlCl_3$ electrolyte (Figure 6.4 d). The measurement always shows a continuous discharge process at -0.4 V, which is likely related to some unknown side reactions of the electrolyte. Interestingly, the measurements could be performed at higher current densities as shown in Figure 6.4 e, f. Similarly, the charge/discharge measurement is very fast in 0.1 M $AlCl_3$ aqueous electrolyte at current density of 0.3 Ag^{-1} (Figure 6.4 h). These outcomes signify the importance of optimization of electrolytes for Al^{3+}-ion insertion.

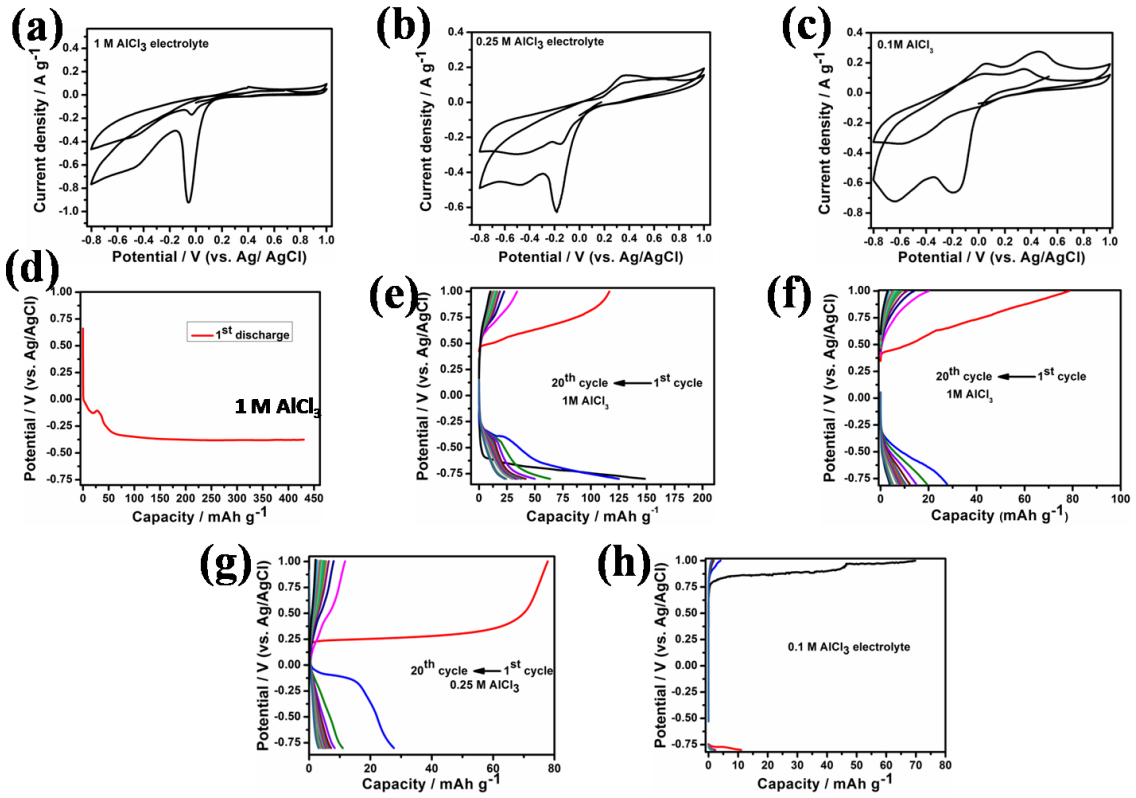

Figure 6.4: CV profile of $LiFePO_4$ at scan rate of 1 mVs^{-1} in (a) 1 M $AlCl_3$, (b) 0.25 M $AlCl_3$, (c) 0.1 M $AlCl_3$ aqueous electrolytes; GCD of $LiFePO_4$ in 1 M $AlCl_3$ aqueous electrolyte at (d) current density of 0.3 Ag^{-1}, (e) current density of 0.75 Ag^{-1}, (f) current density of 1 Ag^{-1}; GCD profile at current density of 0.3 Ag^{-1} in (g) 0.25 M $AlCl_3$, (h) 0.1 M $AlCl_3$ aqueous electrolyte.

We also studied the electrochemical activity of $LiFePO_4$ in 1 M $Al_2(SO_4)_3$ and 1 M $Al(NO_3)_3$ aqueous electrolytes. The charge/discharge profiles (Figure 6.5 a) obtained in 1 M $Al_2(SO_4)_3$ electrolyte is almost similar to the profiles obtained in 0.5 M $AlCl_3$ aqueous electrolyte. The potential plateaus are consistent. However, the specific capacity values are much lower than the 0.5 M $AlCl_3$ aqueous electrolyte. The initial discharge capacity is 33.7 $mAhg^{-1}$ at current density of 0.3 Ag^{-1}. On the other hand, the electrochemical activity of $LiFePO_4$ in $Al(NO_3)_3$ electrolyte is slightly different. There are no noticeable potential plateaus in both charge and discharge cycles and the specific capacities are extremely low (Figure 6.5 b). It also shows high polarization.

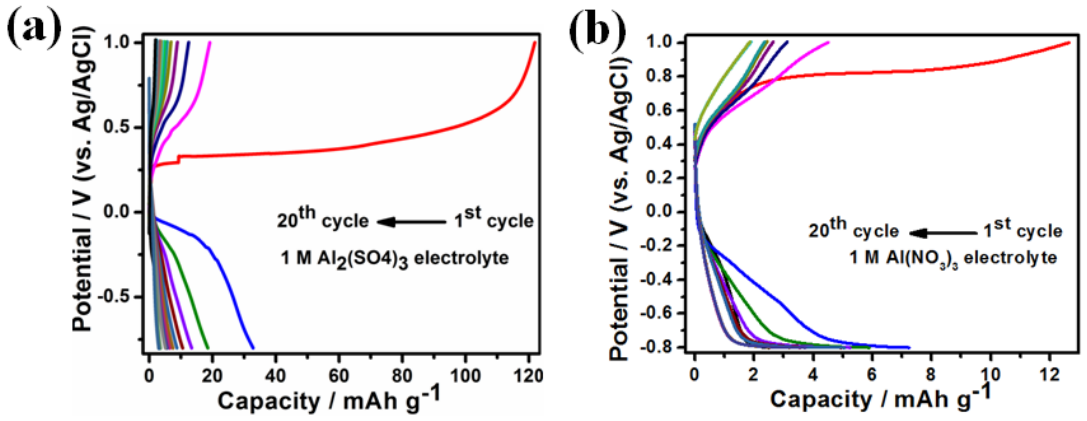

Figure 6.5: GCD profile of $LiFePO_4$ in current density of 0.3 Ag^{-1} in (a) 1 M $Al_2(SO)_4$, and (b) 1 M $Al(NO_3)_3$ aqueous electrolytes.

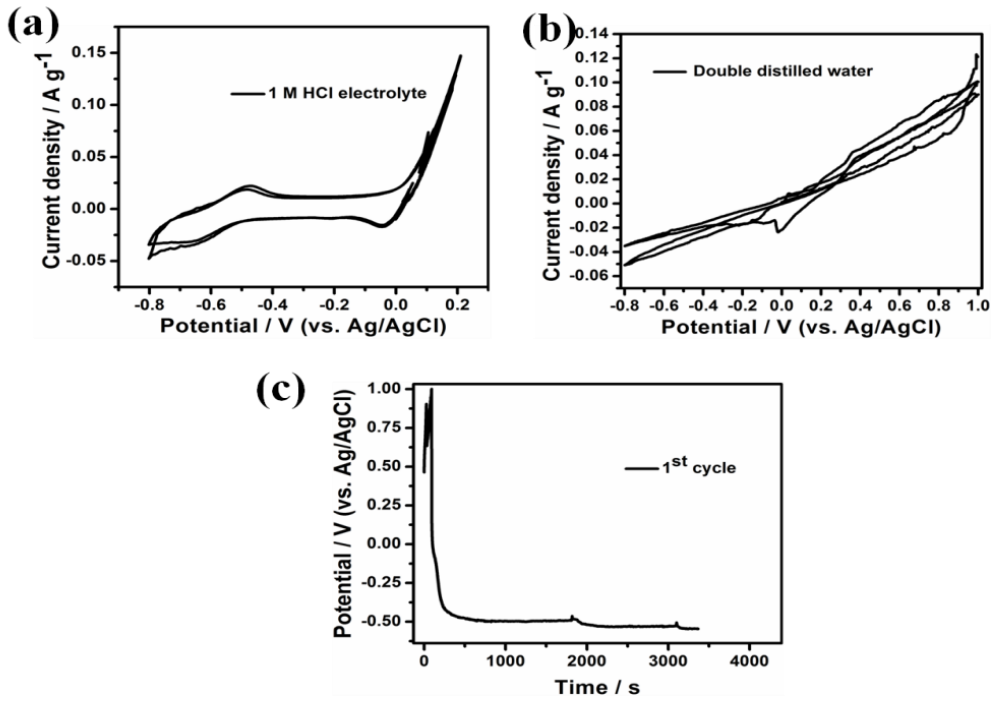

Figure 6.6: CV measurement of $LiFePO_4$ at scan rate of 1 mV s^{-1} in (a) 1 M HCl, (b) pristine water; (c) GCD at current density of 0.3 Ag^{-1} in 1 M HCl aqueous electrolyte.

Since the electrochemical activities are investigated in water-based electrolytes, in order to examine the contribution of any proton intercalation in $LiFePO_4$, CV and charge/discharge experiments were performed in 1 M HCl and pristine water (Figure 6.6). It is seen that there is no noticeable electrochemical activity in these cases which signifies no proton involvement in the study.

To understand the phase transformation upon the electrochemical activity of Al^{3+} ion in $LiFePO_4$ during discharge and charge processes, the cycled electrodes

were interrogated by *ex-situ* electron microcopy and spectroscopy techniques. *Ex-situ* FESEM images, as shown in Figure 6.7 (a-c), of the $LiFePO_4$ electrodes after 1st discharge and 1st charge show no evidence of noticeable disintegration of the electrode upon Al^{3+}-ion reactivity. This is in contrary to the report on $LiMn_2O_4$ electrode where complete disintegration of the electrode was seen during the 1st discharge cycle itself [10].

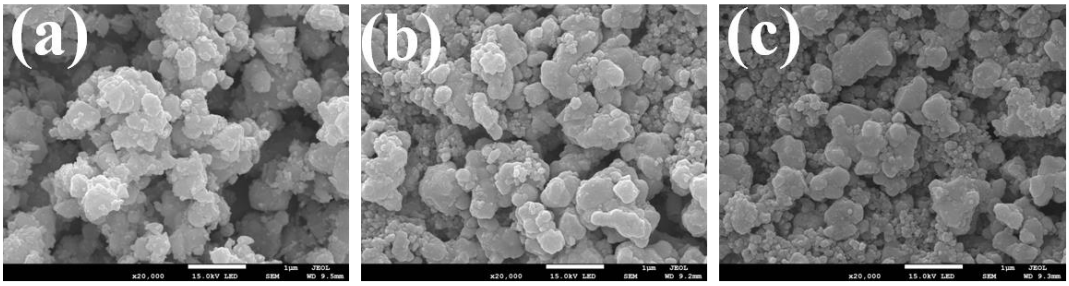

Figure 6.7: *Ex-situ* FESEM of $LiFePO_4$ (a) pristine electrode, (b) after 1st charge, (c) after 1st discharge.

However, certain changes are noticeable in the *ex-situ* XRD patterns. Figure 6.8 shows the *ex-situ* XRD patterns of $LiFePO_4$ electrodes after 1st discharge, 1st charge and 2nd discharge cycles along with the XRD pattern of pristine $LiFePO_4$. The XRD profiles were analyzed with High Score-Plus software (Figure 6.9). It appears that the XRD pattern of the electrode after 1st discharge cycle is almost similar to the pristine $LiFePO_4$ except emergence of two sharp peaks at $2\theta = 38.3^{o}$ and 40^{o} which could be attributed to the presence of Fe_2O_3 (ICSD-98-005-1122). The XRD pattern is also similar to $Al_{0.031}Li_{0.969}FePO_4$ phase (ICSD- 98-016-0778). Quantification analysis suggests the existence of 41% of $Al_{0.031}Li_{0.969}FePO_4$, 12% of Fe_2O_3 and 47% of $LiFePO_4$ in the electrode after completing the 1st discharge cycle. However, the XRD patterns of 1st charge and 2nd discharge states electrodes are analogous, but slightly different from the 1st discharge state and the pristine $LiFePO_4$. The characteristic XRD peak at $2\theta = 17.28^{o}$ for the pristine $LiFePO_4$ corresponds to the (200) plane of $LiFePO_4$. After 1st charge and 2nd discharge, this particular peak almost disappeared with concomitant emergence of a new XRD peak around $2\theta = 18.11^{o}$. Thereafter, the XRD peaks of the pristine material at $2\theta = 22.76^{o}$ and 24.17^{o} are replaced by a new peak at $2\theta = 23.84^{o}$ for both charge/discharge states. Another peak of $LiFePO_4$ at $2\theta = 29.95^{o}$ almost vanished and three consecutive new peaks appeared at $2\theta = 29.73^{o}$, 30.37^{o} and 30.91^{o} for both charge/discharge stages.

Moreover, the peak intensity of the pristine peak at 2θ = 35.74° decreased significantly for both 1st charge and 2nd discharge state electrodes. The electrochemical reaction mechanism of Li^+-ion in $LiFePO_4$ is an intercalation/deintercalation process and it is well evidenced. On contrary to Li^+-ion insertion mechanism, in case of Al^{3+} ion electrochemical reaction in $LiFePO_4$, ex-situ XRD results suggest that it is not only intercalation/deintercalation but conversion mechanism is also possible. Considering the macroscopic size of the investigated $LiFePO_4$, surface adsorption process is expected to be negligible.

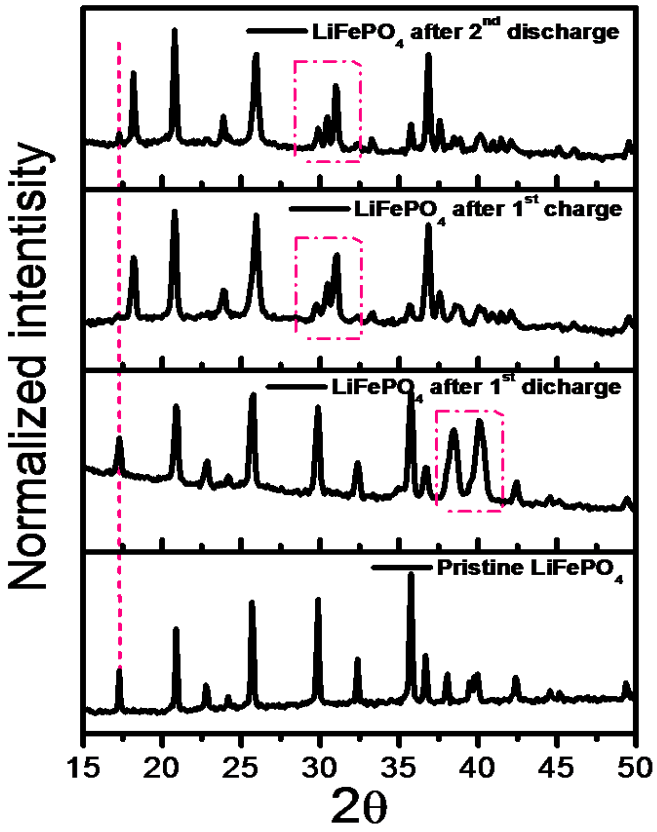

Figure 6.8: *Ex-situ* XRD patterns of pristine $LiFePO_4$ after 1st charge/discharge and 2nd discharge states.

Apart from it, *ex-situ* XPS has also been carried out for the pristine electrode and charge/discharge electrodes and the spectra are depicted in Figure 6.10. As shown in the Figure 6.10 b, aluminum peak could be observed at 75.2 eV for both charged/discharged state and the same is absent for pristine $LiFePO_4$ electrode [12].

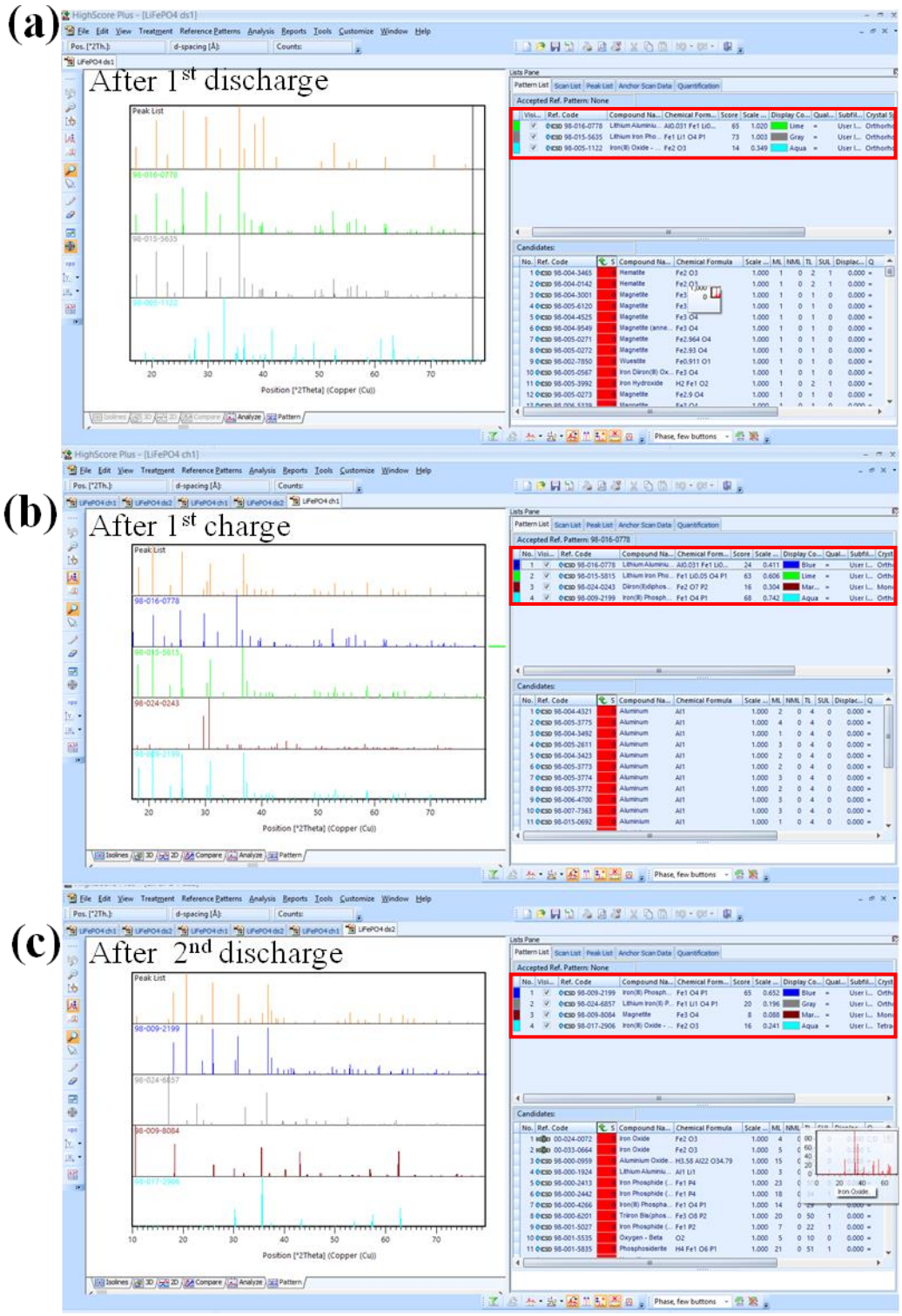

Figure 6.9: (a-c) Screen shot of XRD analysis of HighScore Plus software.

Fe 2P XPS peak (Figure 6.10 c) was analyzed to understand the change in the oxidation states of Fe. As observed from (Figure 6.10 c) Fe 2P spectrum, two main peaks at 711.15 eV for Fe $2p_{3/2}$ and 725eV for Fe $2p_{1/2}$with shake up satellite at

716.53 eV for Fe $2p_{3/2}$ and 730.7 eV for Fe $2p_{1/2}$ could be noticed, which suggests Fe (II) oxidation state in pristine $LiFePO_4$ [13]. The XPS spectrum of the 1st charge cycle (Figure 6.10 c) shows that the main peaks are centered at 712.5 eV and 726.3 eV, which is corresponding to Fe (III) oxidation state [14]. These peaks imply the presence of $FePO_4$ in the electrode after completion of 1st charge process. Again, after completing 1st discharge cycle, XPS peaks are almost similar to pristine electrode. Therefore, Fe(II) states has been recovered after 1st discharged process. XPS spectra of 2P phosphorous (Figure 6.10 e) show a single doublet component attributed to P $2p_{3/2}$ and P $2p_{1/2}$ [15]. The presence of single doublets in all P 2P spectra suggests only one phosphorous environment which signify $(PO_4)^{3-}$ of $LiFePO_4$ [15]. But the global amount of phosphorous was observed continuously decreasing from the pristine electrode to the 1st discharged stage electrode as was revealed from

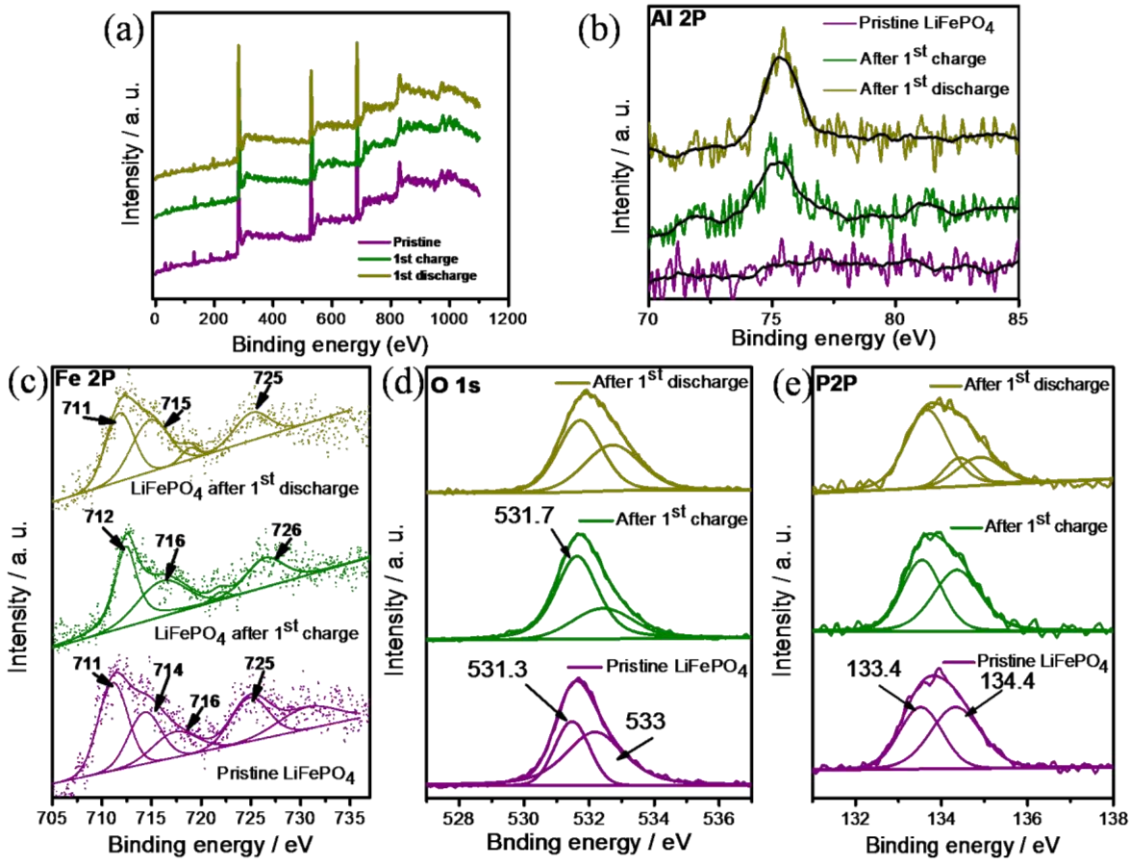

Figure 6.10: *Ex-situ* XPS spectra of (a) summary of pristine and tested electrodes, (b) aluminum 2p spectra, (c) iron 2p spectra, (d) oxygen 1s spectra, and (e) phosphorous 2p spectra for pristine $LiFePO_4$ and after 1st charge/discharge states.

quantitative analysis. Oxygen 1s spectrum shows (figure 6.10 d) that XPS peak at 531.3 eV for pristine electrode attributed to oxygen present in the phosphate group ($(PO_4)^{3-}$). This peak has been shifted to slightly higher binding position (531.7 eV) for the electrodes after 1st charge and discharge. This slight shift of binding energy may result from the accumulation of auxiliary oxygenated species on the electrode surface [15].

Based on the electrochemical outcome and post-mortem analysis of the electrodes, it could be inferred that there is a possibility of Al^{3+}-ion electrochemically reacting with $LiFePO_4$. However, it also appears that structural Li^+-ion also plays a significant role in the charge-discharge process. A comparison of the charge discharge curves, as shown in Figure 6.2 b and Figure 6.2 d, indicates that the features of charge

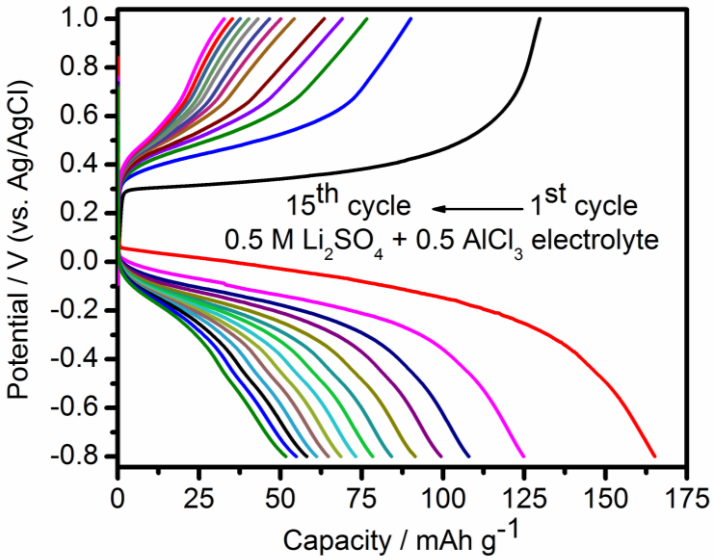

Figure 6.11: GCD profile in mixture of 0.5M Li_2SO_4 and 0.5 M $AlCl_3$ (1:1) aqueous electrolyte of $LiFePO_4$ at current density of 0.3 Ag^{-1}.

and discharge profiles are almost identical for both Li^+-ion and Al^{3+}-ion conducting aqueous electrolytes. First, there is gradual decline of specific capacities in both cases. Second, the charge/discharge potential plateaus in both cases are almost coinciding with each other. However, a close inspection indicates that a polarization value of 0.42 V is seen in the case of Al^{3+}-ion conducting aqueous electrolyte, whereas it is 0.14 V for the Li^+ ion counterpart. Experiments were performed in an aqueous electrolyte with a mixture (1:1 v/v) of 0.5 M Li_2SO_4 and 0.5 M $AlCl_3$. As shown in Figure 6.11, it could be seen that the polarization value in this case is 0.3 V which is

an intermediate value of pristine 0.5 M Li_2SO_4 and 0.5 M $AlCl_3$ electrolytes. Moreover, the charge discharge profiles also shift to higher and lower potential plateaus during respective subsequent charging and discharging cycles similar to the charge/discharge profiles as obtained at pristine 0.5 M $AlCl_3$ electrolyte. This signifies the difficulty in Al^{3+}-ion insertion and extraction from $LiFePO_4$. This is in contrary to $LiMn_2O_4$ study where the charge and discharge potential plateaus are almost superimposed on each other in subsequent cycles [10]. The 1st discharge cycle in case of $LiMn_2O_4$ is completely different from its subsequent cycles and it also leads to disintegration of the electrode with concomitant formation of MnO_2. Such behavior could not be seen at all in case of $LiFePO_4$. It appears that Li^+-ion intercalation and deintercalation take place in case of $LiFePO_4$ even in Al^{3+} conducting aqueous electrolyte.

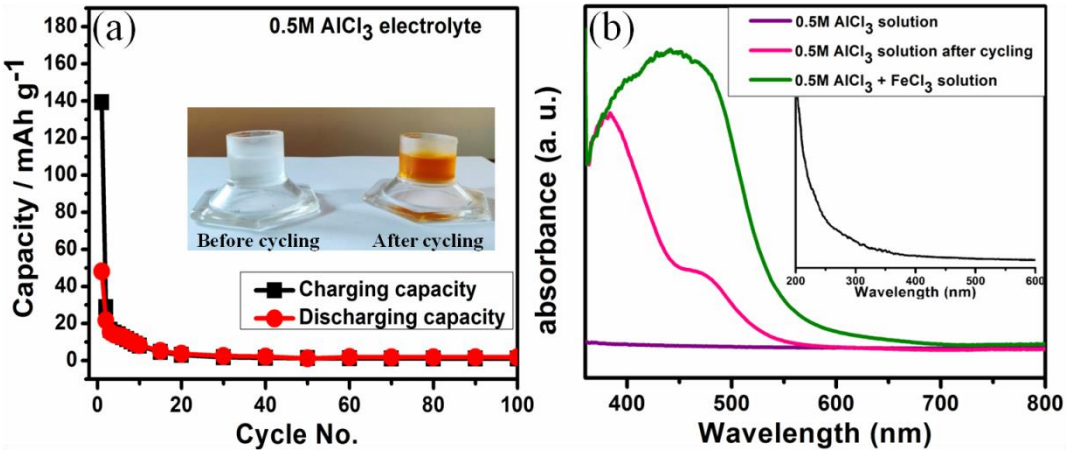

Figure 6.12: (a) Capacity vs. cycle number plot of $LiFePO_4$ in 0.5 M $AlCl_3$ aqueous electrolyte at current density of 1 Ag^{-1}, inset shows the color change of the electrolyte after cycling, and (b) UV-Visible spectra of the electrolytes before and after GCD cycling, inset shows the UV-Visible spectrum of 0.5 M $AlCl_3$ from 200 nm to 600 nm.

The cycling stability of the $LiFePO_4$ electrode is also investigated. It is observed that $LiFePO_4$ shows a charge capacity of 139 $mAhg^{-1}$ and discharge capacity of 48 $mAhg^{-1}$ in the first cycle in 0.5 M $AlCl_3$ electrolyte at the current density of 1 Ag^{-1} (figure 6.12 a). Later on, the electrode exhibits poor capacity retention. The electrode stability has also been tested in other concentration of aqueous $AlCl_3$ electrolyte (such as 0.25 M and 0.1 M) and it is found that 0.5 M electrolyte shows

better electrochemical activity in comparison to the rest of the concentrations. It was found that the color of the $AlCl_3$ electrolyte changes from colorless to orange while performing the experiments all the time as shown in the inset of Figure 6.12 a. Therefore, the electrolyte was analyzed with UV-Visible spectroscopy. As shown in Figure 6.12 b, UV-Visible spectrum of pristine 0.5 M $AlCl_3$ electrolyte indicates having absorption peak in the range of 200-300 nm. However, the UV-Visible spectrum of the same electrolyte after 100 charge/discharge cycles with $LiFePO_4$ electrode exhibits two broad peaks around 380 nm and 470 nm. The change of color of the electrolyte to orange may indicates existence of iron species in the electrolyte.

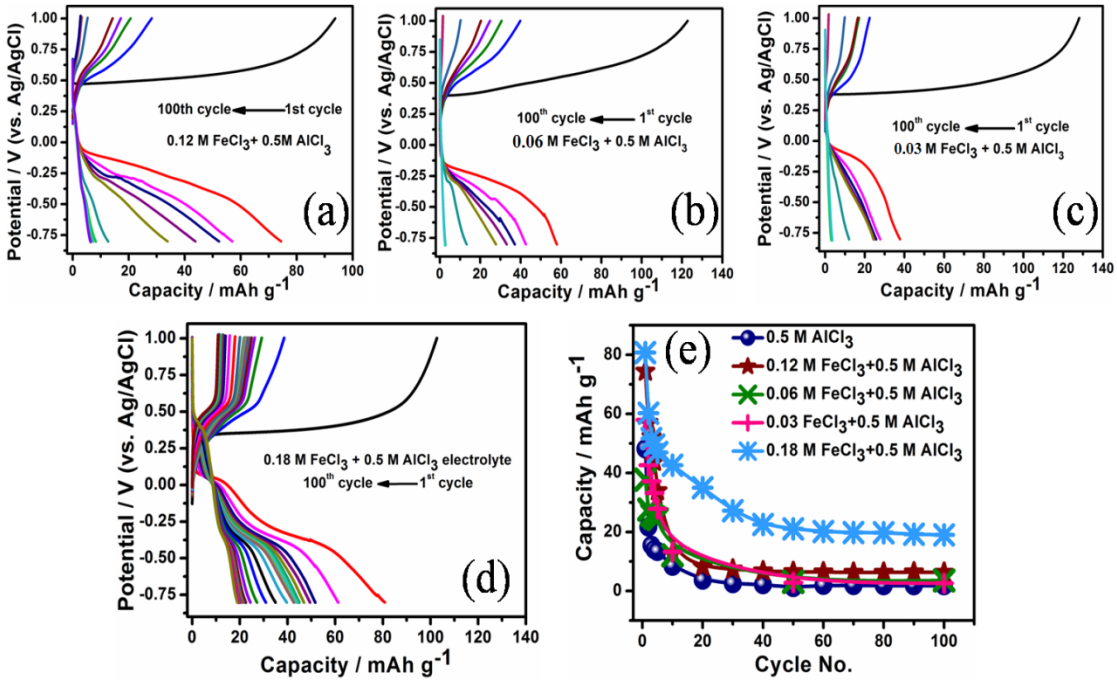

Figure 6.13: GCD profile of $LiFePO_4$ at current density of 1 Ag^{-1} in (a) 0.12 M $FeCl_3$ added in 0.5 M $AlCl_3$, (b) 0.06 M $FeCl_3$ added in 0.5 M $AlCl_3$, (c) 0.03 M $FeCl_3$ added in 0.5 M $AlCl_3$, (d) 0.18 M $FeCl_3$ added in 0.5 M $AlCl_3$ aqueous electrolyte and (e) Capacity retention vs. cycle number plot of $LiFePO_4$ in different concentrations of $FeCl_3$ added in 0.5 M $AlCl_3$ aqueous electrolyte at the current density of 1 Ag^{-1}.

Therefore, we compared the result with the UV-Visible spectrum of (concentration 0.18 M) $FeCl_3$ dissolved in $AlCl_3$ electrolyte and observed a broad peak which is almost superimposing in the same range of electrolyte after discharge. On hindsight, we decided to add certain fraction of $FeCl_3$ in 0.5 M $AlCl_3$ aqueous electrolyte and performed electrochemical experiments. Experiments have been performed in

different concentrations of $FeCl_3$ such as 0.18 M (Figure 6.13 d), 0.12 M (Figure 6.13 a), 0.06 M (Figure 6.13 b), and 0.03 M (Figure 6.13 c). Improvements in specific capacities could be noticed upon addition of $FeCl_3$ in the electrolyte. The capacity versus cycle number plot (shown in Figure 6.13 e) indicates that $LiFePO_4$ could retain discharge capacity of 19 $mAhg^{-1}$ at the 100^{th} cycle in 0.18 M $FeCl_3$ added $AlCl_3$ electrolyte, whereas this value is only 2.63 $mAhg^{-1}$ for 0.03 M $FeCl_3$ added $AlCl_3$ electrolyte and 1.8 $mAhg^{-1}$ for pristine $AlCl_3$ electrolyte. The measured current density was identical in all cases (1 Ag^{-1}). It signifies that there is possibility of leaching of iron species from the electrode in the electrolyte. This enhancement in specific capacities signifies the scope for improving the electrochemical performance of $LiFePO_4$ by optimization of the electrolytes. It is noted here that we could not perform experiments beyond 0.18 M $FeCl_3$ due to deposition of orange colored byproduct in the counter electrode.

6.4 Conclusion

In summary, the Al^{3+} ion electrochemical behavior of $LiFePO_4$ in aqueous electrolyte is illustrated. The electrochemical and post-mortem analysis reveal that a complex electrochemical mechanism undergoes while Al^{3+}-ion reacts with $LiFePO_4$. While specific capacity decline was observed during cycling, it was shown that it could be mitigated by optimization of the electrolyte. In this context, addition of iron chloride in the electrolyte could stabilize the cycling profiles by almost 23.5 %.

6.5 References

[1] Padhi, A.K., Nanjundaswamy, K.S., and Goodenough, J.B. Phospho-olivines as positive electrode materials for rechargeable lithium batteries. *Journal of the electrochemical society*, 144(4): 1188, 1997.

[2] Sauvage, F., Tarascon, J.M., and Baudrin, E. Insights into the potentiometric response behaviour vs. Li^+ of $LiFePO_4$ thin films in aqueous medium. *Analytica chimica acta*, 622(1-2): 163-168, 2008.

[3] Manickam, M., Singh, P., Thurgate, S., and Prince, K. Redox behavior and surface characterization of $LiFePO_4$ in lithium hydroxide electrolyte. *Journal of power sources*, 158(1): 646-649, 2006.

[4] Noerochim, L., Yurwendra, A.O., and Susanti, D. Effect of carbon coating on the electrochemical performance of $LiFePO_4$/C as cathode materials for aqueous electrolyte lithium-ion battery. *Ionics*, *22*(3): 341-346, 2016.

[5] Mi, C.H., Zhang, X.G., and Li, H.L. Electrochemical behaviors of solid LiFePO4 and $Li_{0.99}Nb_{0.01}FePO_4$ in Li_2SO_4 aqueous electrolyte. *Journal of Electroanalytical Chemistry*, 602(2): 245-254, 2007.

[6] Vujković, M., Stojković, I., Cvjetićanin, N., and Mentus, S. Gel-combustion synthesis of $LiFePO_4$/C composite with improved capacity retention in aerated aqueous electrolyte solution. *Electrochimica Acta*, 92: 248-256, 2013.

[7] Manjunatha, H., Venkatesha, T.V., and Suresh, G.S. Kinetics of electrochemical insertion of lithium ion into $LiFePO_4$ from aqueous 2 M Li_2SO_4 solution studied by potentiostatic intermittent titration technique. *Electrochimica acta*, 58: 247-257, 2011.

[8] He, P., Zhang, X., Wang, Y.G., Cheng, L., and Xia, Y.Y. Lithium-ion intercalation behavior of $LiFePO_4$ in aqueous and nonaqueous electrolyte solutions. *Journal of the Electrochemical Society*, *155*(2): 144, 2007.

[9] Love, C.T., Korovina, A., Patridge, C.J., Swider-Lyons, K.E., Twigg, M.E., and Ramaker, D.E. Review of $LiFePO_4$ phase transition mechanisms and new observations from x-ray absorption spectroscopy. *Journal of The Electrochemical Society*, 160(5): A3153, 2013.

[10] Nandi, S., and Das, S.K. An electrochemical study on $LiMn_2O_4$ for Al^{3+} ion storage in aqueous electrolytes. *Physical Chemistry Chemical Physics*, 23(35): 19150-19154, 2021.

[11] He, P., Liu, J.L., Cui, W.J., Luo, J.Y., and Xia, Y.Y. Investigation on capacity fading of $LiFePO_4$ in aqueous electrolyte. *Electrochimica acta*, 56(5): 2351-2357, 2011.

[12] González, J.R., Nacimiento, F., Cabello, M., Alcántara, R., Lavela, P., and Tirado, J.L. Reversible intercalation of aluminium into vanadium pentoxide xerogel for aqueous rechargeable batteries. *RSC advances*, 6(67): 62157-62164, 2016.

[13] Castro, L., Dedryvère, R., Ledeuil, J.B., Bréger, J., Tessier, C., and Gonbeau, D. Aging mechanisms of $LiFePO_4$//graphite cells studied by XPS: redox

reaction and electrode/electrolyte interfaces. *Journal of The Electrochemical Society*, 159(4): A357, 2012.

[14] Yamashita, T., and Hayes, P. Analysis of XPS spectra of Fe^{2+} and Fe^{3+} ions in oxide materials. *Applied surface science*, 254(8): 2441-2449, 2008.

[15] Castro, L., Dedryvere, R., El Khalifi, M., Lippens, P.E., Bréger, J., Tessier, C., and Gonbeau, D. The spin-polarized electronic structure of $LiFePO_4$ and $FePO_4$ evidenced by in-lab XPS. *The Journal of Physical Chemistry C*, 114(41): 17995-18000, 2010.